IEEE Photonics Journal
An IEEE Photonics Society Publication

Open Access

Transmission Matrix Based Image Super-Resolution Reconstruction Through Scattering Media

Volume 12, Number 3, June 2020

Shenghang Zhou
Xiubao Sui
Yingzi Hua
Qian Chen
Guohua Gu
Hongyang Bai

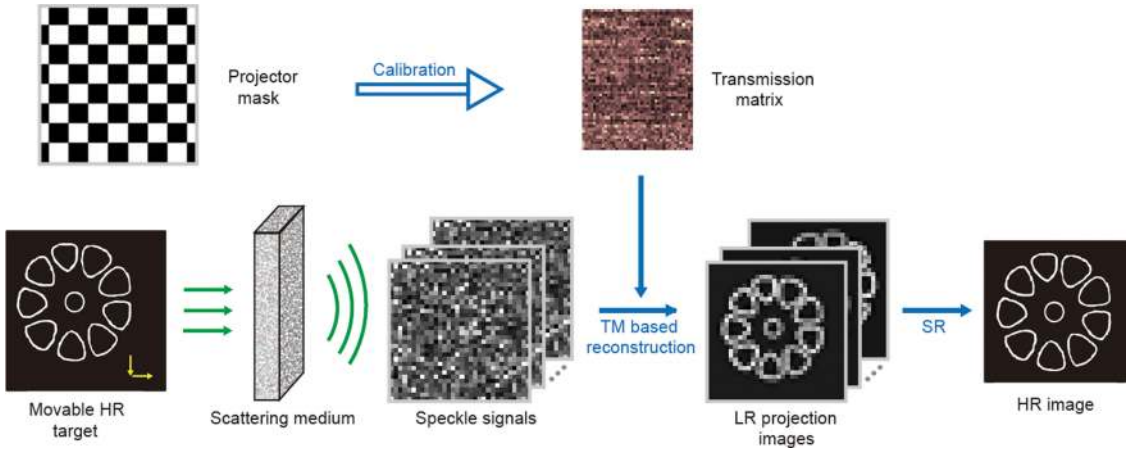

DOI: 10.1109/JPHOT.2020.2988405

IEEE photonics SOCIETY
IEEE

Transmission Matrix Based Image Super-Resolution Reconstruction Through Scattering Media

Shenghang Zhou,[1] Xiubao Sui,[1] Yingzi Hua,[1] Qian Chen,[1] Guohua Gu,[1] and Hongyang Bai[2]

[1]School of Electronic Engineering and Optoelectronic Technology, Nanjing University of Science and Technology, Nanjing 210094, China
[2]School of Energy and Power Engineering, Nanjing University of Science and Technology, Nanjing 210094, China

DOI:10.1109/JPHOT.2020.2988405

Manuscript received February 21, 2020; revised April 12, 2020; accepted April 13, 2020. Date of publication April 20, 2020; date of current version May 26, 2020. This work was supported in part by the National Natural Science Foundation of China under Grants 11773018 and 61727802, in part by Key Research & Development programs in Jiangsu China under Grant BE2018126in part by Fundamental Research Funds for the Central Universities under Grant 30919011401 and 30920010001, and in part by Leading Technology of Jiangsu Basic Research Plan under Grant BK20192003. Corresponding author: Xiubao Sui (e-mail: sxbhandsome@163.com).

Abstract: Measuring optical transmission matrix has enabled image detection through scattering media, however its retrieved resolution is severely limited by the number of measurements. In this paper, we introduce super resolution reconstruction into transmission matrix based imaging scheme, to some extent bypassed this limitation. We demonstrate all detailed information of high-resolution subpixel shifting target are preserved in its corresponding speckle signals. And through phase conjugate reconstruction one can get target's low-resolution projection images with accuracy. The final high-resolution image is achieved by subpixel registration and bilinear interpolation operations. The feasibility of the proposed method is theoretically analyzed and proved by laboratory experiments.

Index Terms: Scattering medium, super-resolution imaging, transmission matrix.

1. Introduction

Light wave propagation through materials with refractive index heterogeneities suffer from strongly scattering, which invalidate traditional imaging methods. In recent years there has been a series of new-style methods, by use of scattered lights rather than ballistic lights, achieved image detection through scattering media. For example, wave-front shaping based focusing [1], memory-effect based method [2], and measuring the media's input-output responses – the transmission matrix (TM). The optical TM was first explored by Popoff et. al [3], and then extended for image detection through opaque materials [4]. Measuring a TM transform an opaque sample as a linear optical system thus enable object's reconstruction from its scattered field. However, to calibrate a system for its TM requires both the scanning of input modes and the recording of each input mode's complex field at the output. This process is rather time-consuming thus during that needs the scattering sample stay stable. Considering the retrieved resolution is equivalent to the number of calibrated input modes [4], TM based imaging methods must trade off the measurement time and the reconstructed resolution. That's one major reason why they only have been applied successfully

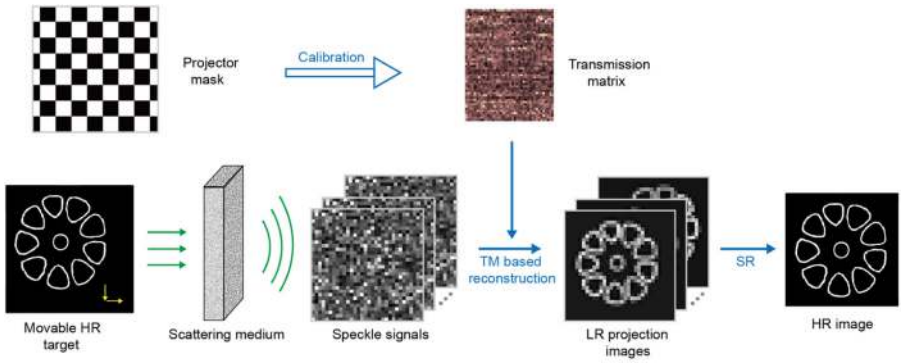

Fig. 1 Schematic of proposed TM based SR reconstruction.

for static materials, for example a diffuser [5] or white paint [3], [4], [6], and failed in dynamic materials (e.g., tissue) [7]. To deal with the resolution issue, many researches have tried to speed up the calibration process by adopting more advanced modulator, such as digital micromirror device (DMD) [8], [9], but the problem still exists.

As to traditional lens-based imaging applications, there are also a persistent need for high spatial resolution. The most commonly hard-ware based way is to increase the number of pixels per unit region of the detector. It's not always effective because decreasing the pixel size reduce the amount of lights reaching single pixel, which will induce more shot noise and so that the image quality will be degraded. Another effective way is the resolution enhancement, often cited as super-resolution (SR) reconstruction, which aims to obtain high-resolution (HR) image from single or multi low-resolution (LR) images. For decades, the multiple images way [10]–[12] has attract the most attentions. If the used target is movable or by use of extra micrometric displacement device, with relative subpixel shifting, there will be complementary information preserved in LR images. And one can achieved HR image from LR images by algorithms, for example interpolation [13], wiener filter [14], [15] and learning based methods [16], [17].

In this paper, for the first time to our best knowledge, we introduce multi-images SR into TM based imaging scheme, to some extent bypassed the trade-off between the measurement time and the retrieved resolution. For simplicity, our method is named TM based SR reconstruction, described as Fig. 1. As shown, a movable HR target with subpixel shifts contribute to multiple speckle signals. LR projection images are obtained through TM based reconstructions. The used single TM is calibrated by using a LR projector mask. The final HR image is achieved by a purposed SR operation. In our method, the subpixel shifts are achieved by loading HR patterns with different subpixel shift factors onto the spatial light modulator (SLM). We demonstrate TM based phase conjugate operation can get LR projection image of the original HR target, with accurate complementary information preserved in. By means of formula derivation, the modified observation model is given. We deal with the signal-to-noise issue by simply increasing the number of chosen CCD pixels and through superimposition. And with the observation model known, we achieve final HR image from LR images by subpixel registration and further bilinear interpolation operations.

The rest of this paper is organized as follows: in Section 2, we show the principle of the proposed TM based SR reconstruction and offer its detailed operations. In Section 3 we offer the experimental results and evaluate the performance. We make a discussion and conclude this paper in Section 4.

2. Principle

2.1 Background

Monochromatic lights propagation through a complex media can be described as a matrix T, of $M \times N$, in which each element t_{mn} links nth of N input mode and mth of M output mode, given by

$$E_m^{out} = \sum_n t_{mn} E_n^{in} \tag{1}$$

Where E_n^{in} and E_m^{out} are the average light fields on the modes at input and output respectively. Usually, a T is obtained by phase-shifting interferometry [3], through controlling the input and measuring the output. Typically, N_{slm}/N adjacent pixels of the used SLM are controlled as a single macro pixel which indicates an input mode. The N_{slm} is the total number of SLM pixels in the controlling part. Correspondingly, each used CCD pixel denotes an output mode. With a T obtained, one can reconstruct the original target from its scattered speckle signal. The retrieved resolution has been determined and thus limited by N [4], and the achieved ratio of signal-to-noise (SNR) is proportion to the number of M [3], [18].

In traditional imaging system, HR target is projected onto the detector plane by lens. Then the distorted projection image is down-sampled and saved by sensor arrays. The observation model [10] can be expressed as

$$Y_{(k)} = DB_{(k)} M_{(k)} X \tag{2}$$

where X stands for the HR target, and $Y_{(k)}$ denotes its kth frame LR projection image. The D is a down-sampling matrix operator which has been determined by the distribution of sensor arrays. $B_{(k)}$ represents a blur matrix, and the warp matrix $M_{(k)}$ stands for the kth subpixel shifting. There exists complementary information preserved in multiple $Y_{(k)}s$. Given LR images, according to the observation model, one can chose proper SR algorithm for the final HR image's reconstruction.

2.2 Reconstruction of LR Image

For the scattering system's calibration process, according to Eq. (1), usually lights scattered from nth input macro pixel and collected by mth CCD pixel are simply expressed as one, with its response reads t_{mn}. However, these lights are actually from N_{slm}/N different SLM pixels, scattered independently and finally interfered onto the CCD pixel. Therefore, illuminated by collimated lights, the t_{mn} is given by

$$t_{mn} = \sum_{i \in R_n} t_{mn,i} \Big/ (N_{slm}/N) \tag{3}$$

Where the R_n stands for the region of nth macro pixel with N_{slm}/N SLM pixels included in, the $t_{mn,i}$ stands for the response between the ith SLM pixel which is located in R_n and the mth CCD pixel. Thus, mathematically, the T can be expressed as

$$T = SP^t \tag{4}$$

Where S of $M \times N_{slm}$ denotes a unknow TM of the used system, comprised of all the $t_{mn,i}$s. The S can be thought as a small subset of the real scattering matrix and thus obeying Gaussian random distribution [19], linking N_{slm} independent SLM pixels and M CCD pixels. The P^t is a transposed projector matrix whose format is contributed by the used projector mask. The superscript $.^t$ indicates matrix transposition. The projector mask is used for measuring the TM, comprised of macro pixels, which is a phase pattern loaded on SLM during the calibration process. For example, as seeing in Fig. 2(a), a projector mask of 2×2 macro pixels loaded on a 4×4 SLM, the corresponding transposed 16×4 projector matrix is as shown in Fig. 2(b) (for concision the re-transposed 4×16 projector matrix is showed).

For the process of acquisition of speckle signals, lights from kth subpixel shifted HR target and collected by CCD should be expressed as

$$y_{(k)} = SM_{(k)} x \tag{5}$$

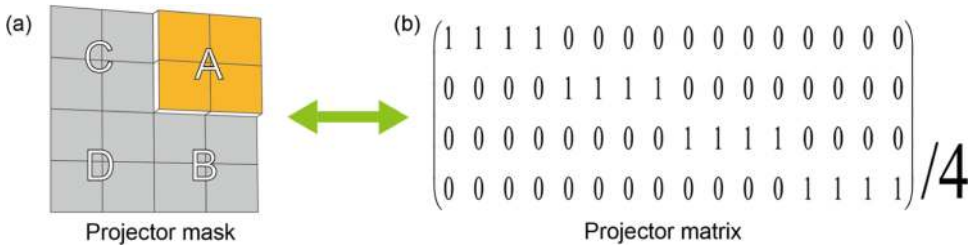

Fig. 2 (a) Projector mask of 2×2 macro pixels loaded on a 4×4 SLM. (b) The corresponding 4×16 re-transposed projector matrix.

Where $y_{(k)}$ is the kth complex-valued $M \times 1$ speckle signal, obtained through interferometry. The target x in this paper stands for a movable virtual pure amplitude object, of $N_{slm} \times 1$ an image vector (actually a $\sqrt{N_{slm}} \times \sqrt{N_{slm}}$ pattern loaded on SLM), realized through subtracting two phase patterns. The $M_{(k)}$ indicates the target's kth subpixel shifting, where the subpixel means partial macro pixel defined by the adopted projector mask.

In the past, only single or multi points [3] or LR patterns [4]–[6] have been used as targets for TM based imaging, and their minimum details are at least matched single input macro pixel. So that directly they could be reconstructed, with accuracy and without resolution loss. We note that, as expressed in Eq. (4) and (5), the calibration process is independent to the acquisition of speckle signals. And at the assumption of ideal optics, all HR details are preserved in the speckle signals without any loss of information.

With respect to the TM based reconstruction, the kth retrieved image can be achieved from the kth speckle signal $y_{(k)}$, given by

$$x_{(k)}^{LR} = T^{\dagger}\, y_{(k)} \tag{6}$$

Here the phase conjugate operator $.^{\dagger}$ is chosen, because $T^{\dagger} = PS^{\dagger}$. According to Eq. (5) and (6), the retrieved image can be expressed as

$$x_{(k)}^{LR} = PS^{\dagger} S M_{(k)} x \tag{7}$$

Considering $S^{\dagger}S \approx I$ due to the character of Gaussian random matrix, according to Eq. (3), the value of nth retrieved element is given by

$$x_{(k)}^{LR}(n) = \sum_{i \in R_n} A_{n,i} e^{i\varphi_{n,i}} / (N_{slm}/N) \tag{8}$$

Where $A_{n,i}$ and $\varphi_{n,i}$ are amplitude and phase of the kth subpixel shifting target, at the location of ith SLM pixel which is located in nth input macro pixel. Given the target is a pure amplitude pattern, the $\varphi_{n,i} \equiv 0$ for $\forall i \in R_n$ and $n \in N$, in other words $e^{i\varphi_{n,i}} \equiv 1$. That is to say, the value of the retrieved $x_{(k)}^{LR}(n)$ is the average of the $A_{n,i}$s for $\forall i \in R_n$. Thus the $x_{(k)}^{LR}$, of $N \times 1$, is a pure amplitude image vector, can be thought as the kth down-sampled LR projection image of the original HR pattern.

Define the blur matrix $B = S^{\dagger} S$, considering Eq. (2) and (7), the modified observation model can be expressed as

$$x_{(k)}^{LR} = PBM_{(k)} x \tag{9}$$

Indeed, the projector matrix P has been used like a typical down-sampling matrix operator as defined in Eq. (2). Differ from traditional lens-based way in which the distorted image is down-sampled by sensor arrays at the CCD plane, in TM based way the reconstructed LR image can be thought as projected onto the SLM plane and down-sampled by the used projector mask. The down-sampling process happen during the TM based reconstruction rather than the signal's acquisition process.

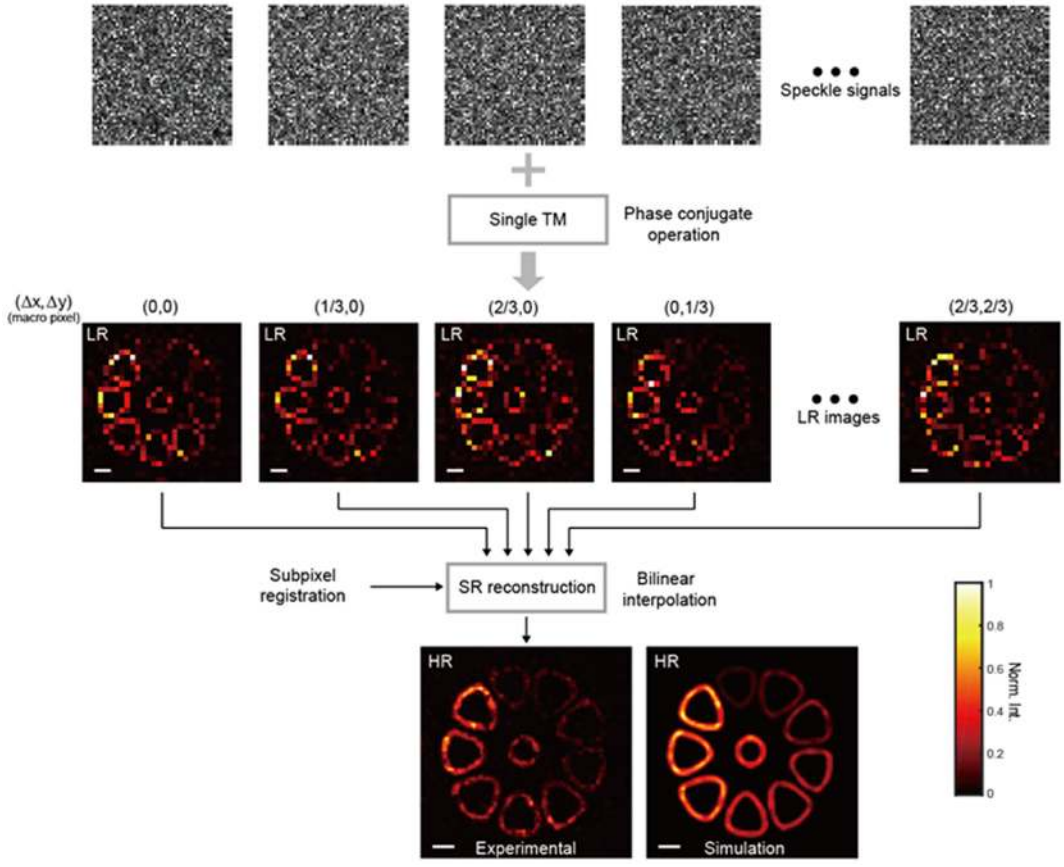

Fig. 3 Schematic of reconstructions of LR images and the final HR image. During phase conjugate operations the sampling rate parameter $\gamma = 10$.

2.3 TM based SR reconstruction

The process of proposed TM based SR reconstruction is as described in Fig. 3. As shown, LR images are reconstructed from speckle signals, through phase conjugate operations by use of single measured TM. The speckle signals are acquired from patterns loaded on SLM, these patterns are of same target and with different subpixel shift factors. The *k*th shift factor is represented by $M_{(k)}$ defined in Eq. (9). Given LR images with observation model known, we achieve final HR image by a proposed SR method. The SR in this paper means the processes of subpixel registration and further bilinear interpolation operation. The detailed operations are as follows. Note that measuring multiple speckle signals will increase the acquisition time, the following multiple TM based reconstructions and further SR operation means the purposed method has a higher computation complexity.

In our method, the subpixel shifting is generated by loading single target's patterns with different translations, both in horizontal and vertical. The shift in horizontal is represented by Δx, and the shift in vertical is expressed by Δy. Values of both Δx and Δy can be 0, $1/3$, or $2/3$. For example as seeing in Fig. 4, a target moved from its original location to a new region, the value of shift factor reads $(\Delta x, \Delta y) = (2/3, 1/3)$. Here, $\Delta x = 2/3$ means the horizontal translation is $2/3$ macro pixel and $\Delta y = 1/3$ indicates the translation in vertical is $1/3$ macro pixel. The format of macro pixels has been defined by projector mask which is used for measuring the TM. Totally, there exist 9 different $(\Delta x, \Delta y)$, correspond to 9 independent speckle signals, and each speckle signal will contribute to a specific LR image through TM based reconstruction. After acquisitions and following computations, we achieve 9 LR images. The further SR operations are as described in Fig. 5.

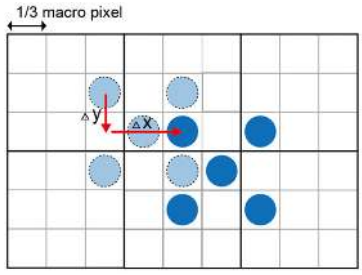

Fig. 4 Schematic diagram of subpixel shifting, a simply movable target as an example. The larger black grids denote macro pixels defined by the used projector mask, while small gray grids indicate the step size of subpixel shifting.

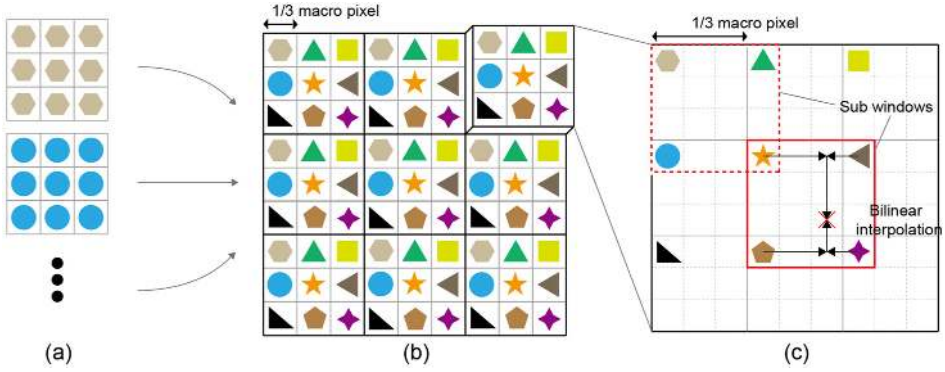

Fig. 5 (a) Schematic of LR image. Each is of 3×3, represented by a specific graph. (b) Result of subpixel registration. The larger black grids and small gray grids denote macro pixels and the step size of subpixel shifting respectively. Blanks between small grids are not shown. (c) Schematic of bilinear interpolation. The showed region is of single macro pixel and comprised of 9×9 resolvable pixels. Every defined sub window is of 4×4 resolvable pixels.

TABLE 1
Different Graphs Denote Different LR Images

$(\triangle x, \triangle y)$	$(0,0)$	$(0,\frac{1}{3})$	$(0,\frac{2}{3})$	$(\frac{1}{3},0)$	$(\frac{1}{3},\frac{1}{3})$	$(\frac{1}{3},\frac{2}{3})$	$(\frac{2}{3},0)$	$(\frac{2}{3},\frac{1}{3})$	$(\frac{2}{3},\frac{2}{3})$
Graph									

In order to explain our method in vivid, we suppose the $N_{slm} = 27 \times 27$ and the adopted projector mask is of 3×3. Therefore, each macro pixel covers 9×9 adjacent resolvable SLM pixels. As discussed above, the sized of retrieved LR images is consistent with the size of projector mask. The values of used shift factors have been showed above, just like Fig. 4. Partial retrieved LR images are as seeing in Fig. 5(a). As shown, information of different LR images with different shift factors are represented by specific graphs. The relationship between shift factors and graphs is given in Table 1.

Because the shifts are already known, we do the subpixel registration by directly putting LR images into HR grids. The arrange of information in HR grids from the 9 LR images are showed in Fig. 5(b), in a simplified form of which blank pixels are not shown. All the 3×3 macro pixel regions are included in Fig. 5(b). The actual region of each macro pixel is as seeing in Fig. 5(c), of 9×9

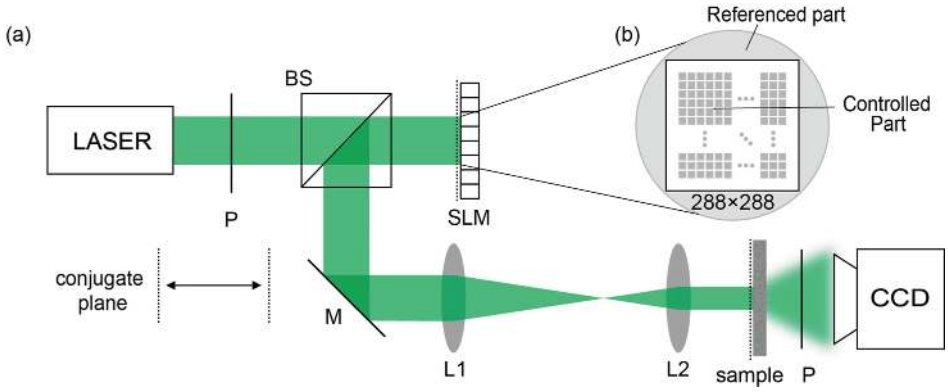

Fig. 6 (a) Schematic of the proposed experimental setup. BS, beam splitter; M, mirror; and P, polarizer. (b) Schematic of illuminated SLM, the controlling part is comprised of 288 $\times$ 288 resolvable pixels.

HR grids. The resolution of all HR grids is equivalent to the original target pattern, in other words 27 $\times$ 27. We fill the blank pixels by bilinear interpolation for the final HR image.

The HR grids are divided into several sub windows, as seeing in Fig. 5(c), each is comprised of 4 $\times$ 4 adjacent resolvable pixels and with 4 registered pixels consisted in. The 4 registered pixels in every sub window are from different LR images. For each macro pixel region there needs 9 sub windows, and totally 81 sub windows are necessary to cover the supposed SLM area. The bilinear interpolation operations are executed in all sub windows sequentially.

In practice, noise is inevitable which will degrade the reconstruction quality. There are reconstruction noise and experimental noise in the proposed method experimentally. The reconstruction noise is included in the modified observation model Eq. (9), expressed as the blur matrix B.The B is unknown, of $N_{slm} \times N_{slm}$, defined by $B = S^{\dagger}_{N_{slm} \times M} \cdot S_{M \times N_{slm}}$. According to the feature of phase conjugate operator discussed in [4], [18], the more M has been used, the B is more approached the identity matrix I. In other words, one can simply increasing M for a better LR reconstruction performance. In the proposed setup, the main experimental noises include the residual amplitude modulation, the optical system distortion and the nonuniform of the used scattering sample. Given the noises are randomized and the retrieved target image is constant, we adopt a simple but effective way for the SNR's improvement. We superimpose multi retrieved LR images each is reconstructed from a shifted target pattern, with different full macro pixel shifting and with the same subpixel shift factor. During that both the reconstruction noise and the experimental noises are averaged and thus eliminated while the target image is held. For example, after 9 superimpositions each LR image's intensity SNR is approximately 9 times than before. The final improved HR images is obtained by SR using these superimposed LR images.

3. Experimental results

The experimental setup is as showed in Fig. 6(a). An expanded monochromatic collimated beam at 532nm is illuminating on a LC-SLM (PLUTO-2-vis-096). As seeing in Fig. 6(b), the SLM's illuminated pixels has been divided into controlling part and referenced part. Both the projector mask and the target pattern are loaded on the controlling part. Lights from the referenced part are used for interferometry. There are 288 $\times$ 288 modulator pixels (the number of N_{slm}) located in the controlling part. A 4-f telescope system with magnification of 0.75 is used to conjugate SLM pixels to points at the entrance of the sample (two stacked diffusers, DG600, Thorlabs). A CCD camera (Point Gray GS3-U3-14S5M-C) is placed 3cm behind the sample's output to record the scattered field.

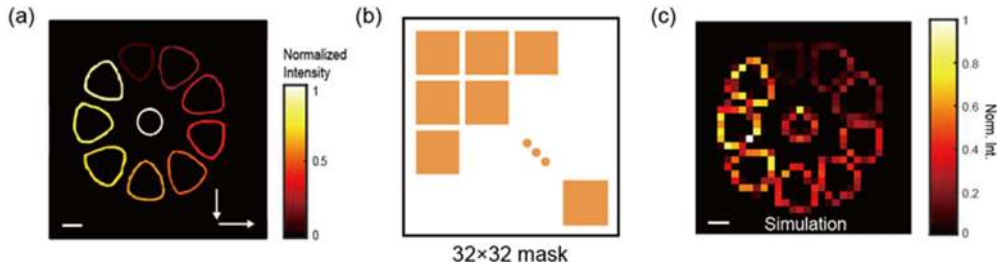

Fig. 7 (a) The original HR target. Pure amplitude pattern with the white arrows indicate the translations in horizontal and vertical. (b) The adopted projector mask for measuring TM. (c) The ideal LR projection image without subpixel shifting from computer simulation.

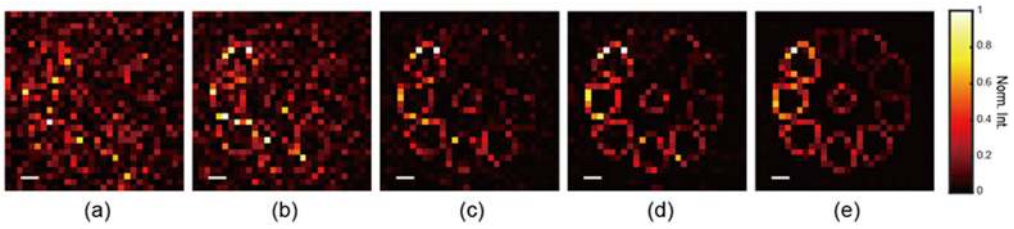

Fig. 8 Experimental results of retrieved LR images. The shift factor $(\Delta x, \Delta y) = (0, 0)$. (a)–(d) are reconstructed with $\gamma = 1$, 2, 5 and 10, respectively. (e) The superimposed result is from 9 frame, all with $\gamma = 10$.

In the rest of this chapter, we first illuminate the used HR target and the adopted projector mask. Then we offer the experimental results of LR images reconstruction and evaluate its performance. The results and performance evaluation of SR are given at last.

The adopted HR target is as seeing in Fig. 7(a), pure amplitude pattern of 288×288, of which different part have gradually enhanced intensity (square of amplitude). The black background indicates region of SLM's controlling part. For the TM's measurement, the used projector mask is as seeing in Fig. 7(b). As shown, every 9×9 adjacent resolvable pixels are controlled as single macro pixel, and totally 32×32 macro pixels cover the entire controlling part. In the object pattern Fig. 7(a) and all following images including the prior Fig. 3, the scale bars mean the same length of 3 macro pixels. The target's ideal LR projection image without subpixel shifting is as seeing in Fig. 7(c), an intensity image (square of obtained pure amplitude pattern) obtained from computer simulation.

In this implement, $N_{slm} = 288 \times 288$, $N = 1024$ by the projector mask. And the number of chosen CCD pixels M which is used for TM based reconstructions is quantified by the sampling rate parameter γ, defined as $\gamma = M/N$. For example, while $\gamma = 10$, the used $M = 10240$. The shift factors in horizontal and vertical Δx and Δy can be 0, $1/3$, or $2/3$, correspond to 9 LR images. With $\gamma = 10$, partial experimental retrieved LR images with different shift factor have been showed in Fig. 3. Given the LR reconstruction performance is concerned with the number of γ and the process of superimposition theoretically, to test that we offer the reconstructed LR images with $(\Delta x, \Delta y) = (0, 0)$ as an instance. With $\gamma = 1$, 2, 5 and 10 without superimposition, the experimental results are showed in Fig. 8(a)–(d), respectively. The superimposition result is as seeing in Fig. 8(e), superimposed from 9 frame full-pixel shifting image each obtained with $\gamma = 10$.

The Pearson Correlation Coefficient (CORR) has been used to evaluate the performance of TM based image detection, while LR pattern is used as target whose resolution matches its projector mask [4]. Value of CORR is calculated between the retrieved image and the original LR pattern. Here, we chose this parameter to quantify the performance of LR reconstructions, by computing the value between the retrieved LR image like Fig. 8 and the ideal LR result from simulation. The

TABLE 2
Relationship Between CORR and γ, for $(\Delta x, \Delta y) = (0, 0)$ with Different γ

γ	1	2	5	10	10 (×9)
CORR	0.4482	0.6389	0.7564	0.8162	0.9421

TABLE 3
Relationship Between CORR and γ, for Different Subpixel Shift Factors with $\gamma = 10$

$(\Delta x, \Delta y)$	$(0,0)$	$(0,1/3)$	$(0,2/3)$	$(1/3,0)$	$(1/3,1/3)$	$(1/3,2/3)$	$(2/3,0)$	$(2/3,1/3)$	$(2/3,2/3)$
CORR	0.8162	0.8130	0.8121	0.8164	0.7816	0.8266	0.7551	0.7918	0.8246

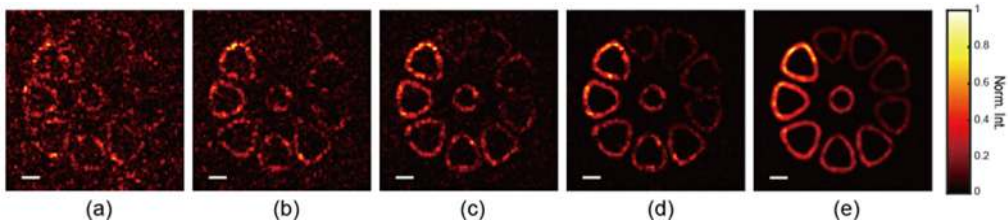

Fig. 9 Experimental results of final retrieved HR images. (a)–(d) are reconstructed from LR images with $\gamma = 1$, 2, 5 and 10, respectively. (e) The result from superimposed LR images, with $\gamma = 10$.

ideal image of Fig. 8 has been showed in Fig. 7(c). We give the CORR values of Fig. 8 in Table 2. Besides, the CORR for LR images with other subpixel shift factors, seeing in Fig. 3, are also given in Table 3. As shown, when γ is increasing, the accurate result emerged gradually. And after superimposition, the CORR run up to 0.9412. The experimental result bear comparison with the ideal result.

The resolution of retrieved LR images is 32×32. As expressed in Fig. 5, we put them into HR grids directly, or say the subpixel registration operation. The resolution of HR grids is 288×288, matching the original pattern, comprised of 1024 macro pixels. Each macro pixel region is of 9×9 HR grids, and with 3×3 sub windows included. Each window is of 4×4 resolvable pixels. Totally 1024×9 sub windows are necessary to cover all HR grids. We execute bilinear interpolation operations in all sub windows for the final HR image. The retrieved HR image is as seeing in Fig. 9. And Fig. 9(a)–(d) correspond to $\gamma = 1$, 2, 5 and 10, respectively. That means, for example $\gamma = 2$ indicates the HR image is reconstructed from 9 LR images, every LR image is reconstructed with $\gamma = 2$ like Fig. 8(b). Fig. 9(e) is reconstructed from superimposed LR images, all superimposed from 9 frame, each with $\gamma = 10$.

In order to evaluate the performance of the final SR results, we introduce the Structural Similarity Index (SSIM) parameter, computed between the retrieved HR image and the original pattern. The SSIM is ranging from 0 to 1, larger SSIM means better performance. The SSIM values of Fig. 9 are offered in Table 4. The SSIM value of ideal simulated result which has been given in Fig. 3 is 0.6048. As shown the performance of superimposed result (SSIM = 0.5874) with $\gamma = 10$ approaches the theoretical value. And in contrast with Fig. 9(d) (SSIM = 0.4709), the superimposed result Fig. 9(e) smoothed the inhomogeneous noise mainly induced by the sample's nonuniform.

TABLE 4
Relationship Between SSIM and Different γ

γ	1	2	5	10	10 (×9)
SSIM	0.0999	0.1263	0.2282	0.4709	0.5874

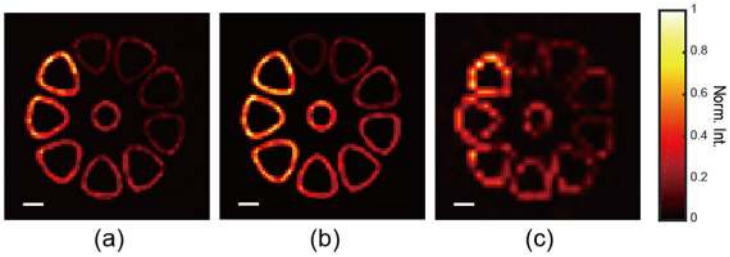

Fig. 10 (a) The experimental result after subpixel registration without bilinear interpolation. (b) The simulation result after subpixel registration without bilinear interpolation. (c) The result of bilinear interpolation without subpixel shifts.

For the SNR issue, both simply increasing M and the superimposition process just act in LR reconstruction processes, therefore finally improve the SR performance. In our method the SR operation is comprised of subpixel registration and the simplest bilinear interpolation. We further discussed the resolution influence of the two processes respectively. Fig. 10(a) is the experimental result of subpixel registration without bilinear interpolation. The achieved image is of resolution 96 $\times$ 96, generated from the 9 superimposed LR projector images each is of resolution 32 $\times$ 32 as shown in Fig. 8(e). The simulation result is in Fig. 10(b) which is directly down-sampled from the original target pattern in Fig. 7(a), also of resolution 96 $\times$ 96. The CORR between these experimental and simulation results is 0.9533. We further compared the result with and without the subpixel shifts. Fig. 10(c) is the straightforward bilinear interpolation result generated from single LR projector image showed in Fig. 8(e). The CORR between Fig. 10(c) and the simulation result Fig. 10(b) is 0.7220, far less than that 0.9533. As shown, through subpixel shifts based TM reconstruction and further subpixel registration operation, the achieved resolution improvement successfully reaches to a factor of 3. In the proposed method, in order to compare SSIM between the final result and the original target pattern, we adopted the bilinear interpolation operation to make the final resolution reach to 288 $\times$ 288 equivalent to that original. It doesn't means our resolution improvement reaches to a factor of 9 exactly. Other popular SR algorithm may perform better than the proposed method.

4. Discussion and conclusion

Among our method the phase conjugate operator has been chosen. Another popular one, the pseudo-inverse operator $.^{-1}$ which has showed theoretical advancement of being able to reconstruct without reconstruction noise at low-level experimental noise [4], [20]. It's not straightforward for unmatched HR target because $T^{-1} \neq PS^{-1}$, referring to Eq. (4). Other TM based reconstruction ways by use of iteration-based algorithms such as OMP [21], TVAL3 [22] and compressive sensing based methods [6], [23] have not been discussed in this paper. In the proposed implement, virtual patterns have been used as the original target, which are loaded on the SLM. For real life target, TM based image detection method has been explored such as detection through single multimode fiber [24], [25]. Our method may be helpful for these TM based uses for a higher resolution performance, while its number of calibrated input modes or say the achieved resolution have not reached fiber's number of resolvable modes. Besides, the purposed setup has a limitation for imaging dynamic

objects, better performance may be achieved by using advanced device such as DMD or through using FPGA instead of computer for controlling.

In this paper, we propose a transmission matrix based image super-resolution reconstruction method. HR patterns loaded on SLM with subpixel shifting factors are used as imaging target. Formula derivation and experimental results show that the images from phase conjugate reconstruction can be thought as LR projection images of the original HR target. The LR images are down-sampled by the adopted projector mask during TM based reconstruction processes. We achieve final HR image by subpixel registration and bilinear interpolation operations. The SNR issue has been discussed. Experimental results show the feasibility of the proposed method.

References

[1] I. M. Vellekoop and A. P. Mosk, "Focusing coherent light through opaque strongly scattering media," *Opt. Lett.*, vol. 32, pp. 2309–2311, Aug. 2007.

[2] O. Katz, E. Small, and Y. Silberberg, "Looking around corners and through thin turbid layers in real time with scattered incoherent light," *Nature Photon.*, vol. 6, pp. 549–553, 2012.

[3] S. M. Popoff, G. Lerosey, R. Carminati, M. Fink, A. C. Boccara, and S. Gigan, "Measuring the transmission matrix in optics: An approach to the study and control of light propagation in disordered media," *Physical Rev. Lett.*, vol. 104, pp. 100601–100604, 2010.

[4] S. Popoff, G. Lerosey, M. Fink, A. C. Boccara, and S. Gigan, "Image transmission through an opaque material," *Nature Commun.*, vol. 1, 2010, doi: 10.1038/ncomms1078.

[5] Y. Zhao, Q. Chen, S. Zhou, G. Gu, and X. Sui, "Super-resolution imaging through scattering medium based on parallel compressed sensing," *IEEE Photon. J.*, vol. 9, 2017, Art. no. 7803012.

[6] A. Liutkus, *et al.*, "Imaging with nature: Compressive imaging using a multiply scattering medium," *Scientific Rep.*, vol. 4, p. 5552, 2014.

[7] M. Kim, W. Choi, Y. Choi, C. Yoon, and W. Choi, "Transmission matrix of a scattering medium and its applications in biophotonics," *Opt. Express*, vol. 23, pp. 12648–12668, 2015.

[8] X. Tao, D. Bodington, M. Reinig, and J. Kubby, "High-speed scanning interferometric focusing by fast measurement of binary transmission matrix for channel demixing," *Opt. Express*, vol. 23, p. 14168, 2015.

[9] A. Drémeau, *et al.*, "Reference-less measurement of the transmission matrix of a highly scattering material using a DMD and phase retrieval techniques," *Opt. Express*, vol. 23, pp. 11898–11911, 2015.

[10] L. Yue, H. Shen, J. Li, Q. Yuan, H. Zhang, and L. Zhang, "Image super-resolution: The techniques, applications, and future," *Signal Process.*, vol. 128, pp. 389–408, 2016.

[11] J. Tian and K. Ma, "Stochastic super-resolution image reconstruction," *J. Vis. commun. Image Representation*, vol. 21, pp. 232–244, 2010.

[12] F. Sina, R. M. Dirk, E. Michael, and M. Peyman, "Fast and robust multiframe super resolution," *IEEE Trans. Image Process.: Publication IEEE Signal Process. Soc.*, vol. 13, pp. 291–294, 2004.

[13] H. Ur and D. Gross, "Improved resolution from subpixel shifted pictures," *CVGIP Graphical Models Image Process.*, vol. 54, pp. 181–186, 1992.

[14] R. Hardie, "A fast image super-resolution algorithm using an adaptive Wiener filter," *IEEE Trans. Image Process.*, vol. 16, pp. 2953–2964, 2007.

[15] R. C. Hardie and K. J. Barnard, "Fast super-resolution using an adaptive Wiener filter with robustness to local motion," *Opt. Express*, vol. 20, pp. 21053–21073, 2012.

[16] Y. Zhao, Q. Chen, X. Sui, and G. Gu, "A novel infrared image super-resolution method based on sparse representation," *Infrared Phys. Technol.*, vol. 71, pp. 506–513, 2017.

[17] L. Kang, C. Hsu, B. Zhuang, C. Lin, and C. Yeh, "Learning-based joint super-resolution and deblocking for a highly compressed image," *IEEE Trans. Multimedia*, vol. 17, pp. 921–934, 2015.

[18] S. M. Popoff, G. Lerosey, M. Fink, A. C. Boccara, and S. Gigan, "Controlling light through optical disordered media: Transmission matrix approach," *New J. Phys.*, vol. 13, pp. 123021–123046, 2011.

[19] C. W. J. Beenakker, "Random-matrix theory of quantum transport," *Physical Rev. Lett.*, vol. 70, p. 1155, 1996.

[20] J. Xu, H. Ruan, Y. Liu, H. Zhou, and C. Yang, "Focusing light through scattering media by trans-mission matrix inversion," *Opt. Express*, vol. 25, pp. 27234–27246, 2017.

[21] J. A. Tropp and A. C. Gilbert, "Signal recovery from random measurements via orthogonal matching pursuit," *IEEE Trans. Inf. Theory*, vol. 53, pp. 4655–4666, 2007.

[22] C. Li, "An efficient algorithm for total variation regularization with applications to the single pixel camera and compressive sensing," M.S. thesis, Rice Univ., 2010.

[23] Y. Zhao, Q. Chen, S. Zhou, G. Gu, and X. Sui, "Super-resolution imaging through scattering medium based on parallel compressed sensing," *IEEE Photon. J.*, vol. 9, 2017, Art. no. 7803012.

[24] Y. Choi, *et al.*, "Scanner-free and widefield endoscopic imaging by using a single multimode optical fiber," *Physical Rev. Lett.*, vol. 109, pp. 203901–203905, 2012.

[25] S. Turtaev, I. T. Leite, T. Altwegg-Boussac, J. M. Pakan, N. L. Rochefort, and T. Čižmár, "High-fidelity multimode fibre-based endoscopy for deep brain in vivo imaging," *Light: Sci. Appl.*, vol. 7, pp. 1–8, 2018.